ARTICLE **OPEN**

Foldable and washable textile-based OLEDs with a multi-functional near-room-temperature encapsulation layer for smart e-textiles

So Yeong Jeong[1,6], Hye Rin Shim[2,6], Yunha Na[1], Ki Suk Kang[1], Yongmin Jeon[1], Seungyeop Choi[1], Eun Gyo Jeong[3], Yong Cheon Park[2], Ha-Eun Cho[1], Junwoo Lee[1], Jeong Hyun Kwon[4], Sung Gap Im [2,5✉] and Kyung Cheol Choi [1✉]

Wearable electronic devices are being developed because of their wide potential applications and user convenience. Among them, wearable organic light emitting diodes (OLEDs) play an important role in visualizing the data signal processed in wearable electronics to humans. In this study, textile-based OLEDs were fabricated and their practical utility was demonstrated. The textile-based OLEDs exhibited a stable operating lifetime under ambient conditions, enough mechanical durability to endure the deformation by the movement of humans, and washability for maintaining its optoelectronic properties even in water condition such as rain, sweat, or washing. In this study, the main technology used to realize this textile-based OLED was multi-functional near-room-temperature encapsulation. The outstanding impermeability of TiO₂ film deposited at near-room-temperature was demonstrated. The internal residual stress in the encapsulation layer was controlled, and the device was capped by highly cross-linked hydrophobic polymer film, providing a highly impermeable, mechanically flexible, and waterproof encapsulation.

npj Flexible Electronics (2021)5:15 ; https://doi.org/10.1038/s41528-021-00112-0

INTRODUCTION

With the emergence of the Internet of Things (IoT), the value of connecting humans and smart electronic devices is increasing. Wearable display devices are interface devices that lead the hyper-connectivity between humans and wearable electronics by visualizing the information processed in wearable electronics to humans. Textile-based display devices can utilize the textile itself as a platform for the display. This ability makes them suitable for daily application in the healthcare, bio-medical, safety, interior, military, and fashion fields[1–5]. Among many display devices, organic light emitting diodes (OLEDs) have achieved significant attention as wearable display devices because of their high flexibility, light weight, low power consumption, and low heat generation. These properties also make them compatible with textile substrates.

In wearable technology, the flexibility of the device is extremely important because the device should not interfere with the active movement of the human body. For this reason, as wearable technology advances, the substrate has increasingly become ultra-thin and ultra-light. However, these properties also seriously reduce the heat resistance of the substrate. In addition, OLEDs also have low thermal stability. To address these problems, the process temperature of the encapsulation film, which is an essential part of water-sensitive OLEDs, should be lowered to near-room-temperature. However, many encapsulation processes are still being conducted at high temperature, around 100 °C.

Chen et al. performed encapsulation at room temperature using CeO₂ and poly(divinylbenzene) (PDVB)[6]. However, the water vapor transmission ratio (WVTR) of that barrier was reported to be 1.81 g m⁻² day⁻¹ at 30 °C and 100% relative humidity (RH) accelerated environments. For the extremely water-sensitive OLEDs, the encapsulation barrier should achieve a WVTR on the order of 10⁻⁶ g⁻² day⁻¹. In addition, the flexibility and waterproof proper-ties of the encapsulation layer were not considered. Wang et al. reported a 2-dyad encapsulation barrier using Al₂O₃ and alucone that was deposited at 50 °C to enhance the reliability of perovskite solar cells[7]. The WVTR of the multi-barrier encapsulation was 1.6×10^{-5} g m⁻² day⁻¹ at 30 °C and 80% RH accelerated environments. The power conversion efficiency (PCE) of the devices was maintained at 96% of initial efficiency for over 2000 h at 30 °C and 80% RH accelerated environments. In order to demonstrate the flexibility of the encapsulation layer, the encapsulation layer was examined by scanning electron microscopy (SEM) after bending 500 times with a 5 mm radius. However, because the purge time of the precursors was over 80 s, it resulted in extremely low throughput. Also, plasma treatment was utilized. Moreover, a bending radius of 5 mm is comparatively large, and 500 bending cycles is insufficient to demonstrate that the barrier has high flexibility. For foldable displays, the required bending radius is 1 mm[8]. The waterproof property of the encapsulation layer was not considered.

The encapsulation film is the most important limitation on the flexibility of the entire textile-based OLED structure, and therefore developing highly flexible textile-based OLEDs typically involves improving the flexibility of the encapsulation layer. Many studies have been performed to achieve this, however, few encapsulation layers have been reported that are capable of enduring a bending strain of more than 1% or a bending radius of less than 5 mm[8] (Supplementary Table 1). In addition, only a few studies have reported on the waterproof property of the encapsulation layer

[1]School of Electrical Engineering, Korea Advanced Institute of Science and Technology (KAIST), Daejeon, Republic of Korea. [2]Department of Chemical and Biomolecular Engineering, Korea Advanced Institute of Science and Technology (KAIST), Daejeon, Republic of Korea. [3]Department of Clothing and Textiles, Chonnam National University, Gwangju, Republic of Korea. [4]Department of Display and Semiconductor Engineering, Sun Moon University, Asan, Republic of Korea. [5]Department of Chemical and Biomolecular Engineering and KI for the NanoCentury, Korea Advanced Institute of Science and Technology (KAIST), Daejeon, Republic of Korea. [6]These authors contributed equally: So Yeong Jeong, Hye Rin Shim. ✉email: sgim@kaist.ac.kr; kyungcc@kaist.ac.kr

and the reported waterproof properties are still less than 200 min (Supplementary Table 2). To realize an environmentally robust textile-based OLED that is durable against wet conditions such as rain, sweat, or washing, an improved waterproof property is required.

In this study, to realize a reliable, foldable, and washable textile-based OLED, a multi-functional encapsulation that simultaneously exhibits an WVTR on the order of 10^{-6} g m^{-2} day^{-1}, high transparency, high curvature flexibility, waterproof property, and a near-room-temperature process was developed. Although the process temperature was only 40 °C, the WVTR of the bilayer encapsulation was estimated to be 9.94×10^{-6} g m^{-2} day^{-1} at 30 °C and 90% RH and its thickness was only 115 nm. In addition, it showed the highest bending performance and waterproof property among reported encapsulation barriers (Supplementary Tables 1 and 2).

By utilizing this multi-functional encapsulation layer, a reliable, foldable, and washable textile-based OLED was realized and its practical utility was demonstrated. The textile-based OLED showed an enhanced operating lifetime of 160 h under ambient conditions. Also, it endured repetitive high curvature bending, maintaining its optoelectronic properties and operating lifetime after tensile bending with a 1.5 mm radius for 1000 repetitions. In addition, the encapsulated OLEDs showed unchanged optoelectronic characteristics even after immersion in water for 1440 min, which suggest its potential for waterproof wearable OLEDs.

RESULTS AND DISCUSSION

Figure 1a illustrates the proposed textile-based OLED and a multi-functional near-room-temperature encapsulation layer. The red phosphorescent OLED (phOLED) was fabricated on a conventional polyester fabric substrate and passivated with a bilayer encapsulation. As shown in Fig. 1b, the bilayer encapsulation was a double-layer structure, where a 1,3,5-trivinyl-1,3,5-trimethyl cyclotrisiloxane (pV3D3) polymer film was deposited on an Al$_2$O$_3$/TiO$_2$ nanolaminate layer (AT nanolaminate layer). The AT nanolaminate is a thin film comprised of alternately deposited Al$_2$O$_3$ and TiO$_2$. By utilizing this multi-functional encapsulation on both the top and bottom sides of the OLED, a real wearable OLED was realized on conventional dress-shirts and T-shirts. The chemical structures of each of the organic layers used in the textile-based OLED with encapsulation layer are shown in Fig. 1c. As shown in Fig. 1d, the wearable OLED emitted red light even when folded under water, as would occur during hand-washing, demonstrating its practical applicability, mechanical durability, and environmental robustness.

High impermeability of the near-room-temperature TiO$_2$ film

An atomic layer deposition (ALD) film is formed by ligand exchanges between the molecules of a metal organic precursor and a reactant precursor. In thermal ALD, as the deposition temperature decreases, the ligand exchange does not occur completely, because the main source of the ligand exchange is thermal energy. For this reason, the higher the deposition temperature, the better the film quality, specifically, it's density or purity, which thereby improves the barrier property[9–11]. Figure 2a indicates that the barrier property of Al$_2$O$_3$ was actually enhanced as the deposition temperature increased[7]. Accordingly, many studies have performed the encapsulation process at a high temperature, around 100 °C. However, such a high-temperature process may cause thermal damage to organic electronic devices with low thermal stability. For example, Fig. 2b shows the operating lifetimes of textile-based OLEDs stored for 3 h at 40, 70, and 100 °C. The data confirm that the higher the storage temperature, the shorter the operating lifetime of the textile-based OLEDs due to detrimental thermal damage. The lifetime of

the device stored at 40 °C was more than twice that of the device stored at 100 °C.

To resolve this problem, TiO$_2$ thin film was deposited at near-room-temperature, and exhibited extremely outstanding impermeability. This demonstration enabled the development of a near-room-temperature encapsulation with low WVTR on the order of 10^{-6} g m^{-2} day^{-1}. As shown in Fig. 2c, the WVTR of TiO$_2$ film deposited at 40 °C was estimated to be 3.17×10^{-5} g m^{-2} day^{-1} at 30 °C and 90% RH acceleration environments, even with a thickness of 30 nm. In fact, the TiO$_2$ thin film exhibited a higher barrier property than Al$_2$O$_3$, which is currently the most commonly used encapsulation material due to its high impermeability. Specifically, the barrier property of a single TiO$_2$ barrier deposited at a near-room-temperature was higher than that of a 2.5-dyad Al$_2$O$_3$ multi-barrier deposited at 120 °C.

The ALD TiO$_2$ film also showed a unique WVTR tendency depending on deposition temperature. As shown in Fig. 2d, the WVTR of the TiO$_2$ film was lowest when deposited at near-room-temperature and rapidly increased as the deposition temperature increased from around 55 °C. This tendency is unlike other ALD films, where the WVTR decreases as deposition temperature increases[7]. In order to specifically clarify why the TiO$_2$ thin film deposited at near-room-temperature had much higher impermeability than the TiO$_2$ thin film deposited at a higher temperature, many film properties including composition, surface roughness, film density, infrared absorption spectrum, and crystallinity were measured (Supplementary Fig. 1). The measurement results obtained for the TiO$_2$ deposited at near-room-temperature were all the same as the results of the TiO$_2$ deposited at a higher temperature. In the measurement results shown in Supplementary Fig. 1, no distinct difference in film properties was observed between the high-temperature and low-temperature deposition samples.

This unique phenomenon of TiO$_2$ is in good agreement with the ALD process window graph (Supplementary Fig. 2a). As shown in Fig. 2e, the ALD process window was located at near-room-temperature, 40–55 °C, where the WVTR was the lowest. The desorption phenomenon began to occur around 55 °C, when the WVTR started to increase rapidly[12–14]. It was determined that because the energy barrier required for ligand exchange between tetrakisdimethylamino titanium (TDMAT) and H$_2$O precursor molecules is low, the high-quality TiO$_2$ film can be formed with only low thermal energy. For this reason, the TiO$_2$ film exhibited outstanding moisture impermeability despite the near-room-temperature process.

In addition, it was notable that the desorption behavior started to occur at a relatively low temperature of about 55 °C[12–14] (Supplementary Fig. 2a and Fig. 2e). The desorption stability of the TDMAT intermediate product is related to the desorption energy barrier D2, which is determined by reaction kinetics, and the energy difference before/after desorption ΔG, which is determined by thermodynamics (Supplementary Fig. 2b). According to density functional theory (DFT), the desorption energy barrier of the TDMAT intermediate product is 1.39 eV and thermodynamically, the desorption behavior is preferred because it is an exothermic reaction[15,16]. These results suggest why the desorption phenomenon of the TDMAT intermediate products occurred at a relatively low temperature.

Theoretically, the reason for the increase in WVTR at high temperature was determined to be the increased residual stress in the film due to continuous desorption phenomenon. It has been reported that the residual stress in ALD films is determined during the growth of the thin film, and that defects or impurities generated during the deposition process can cause high residual stress[17–20]. It has been also reported that the residual stress in Al$_2$O$_3$ films decreased as the deposition temperature increased, because there were fewer precursor residue impurities in the film[17,18]. In the case of TiO$_2$, the bonds of the molecules are
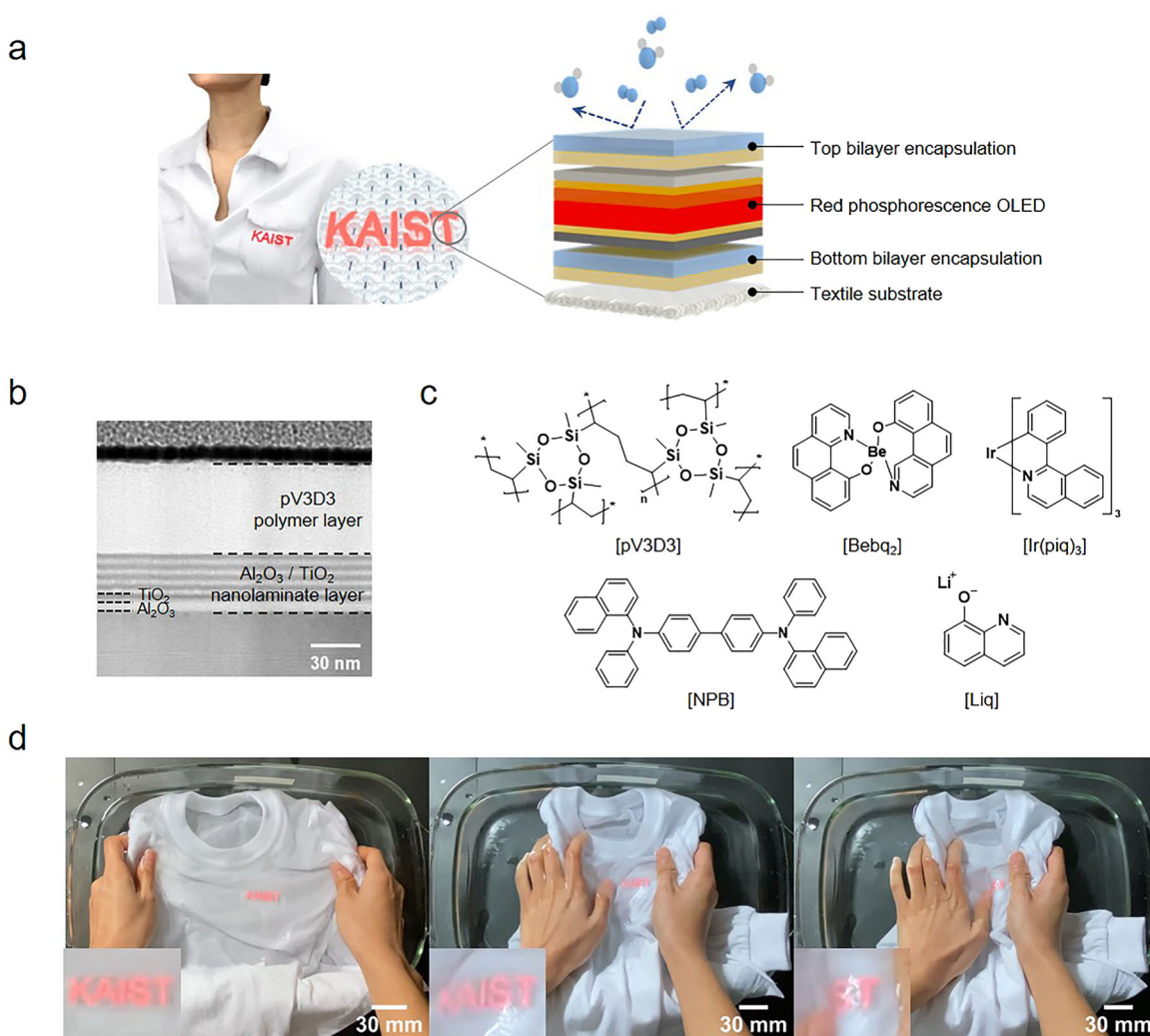
Fig. 1 **Wearable OLED with a multi-functional encapsulation layer. a** Illustration of the proposed textile-based OLED and encapsulation layer. **b** TEM image of the encapsulation layer. Scale bar, 30 nm. **c** Chemical structure of each layer, the polymer capping and host-dopant emitting layer (top), and the hole transport and electron injection layer (bottom). **d** Photographs of the wearable OLED being folded by hand in water. Scale bar, 30 mm.

repeatedly formed and broken due to the continuous desorption phenomenon at high temperature. This desorption behavior during the deposition process can potentially increase the internal residual stress in the film, and this internal residual stress decreased the barrier property. Based on linear elastic fracture mechanics, internal residual stress is an important factor in crack growth[20,21]. The strain energy release rate, G_{ss} is given by

$$G_{ss} = Z\sigma^2 h \left(E_f^*\right)^{-1} \qquad (1)$$

where Z is the dimensionless energy release rate, σ is the residual or applied stress in the film, h is the thickness of the film, and E_f^* is the plane strain elastic modulus. G_{ss} is the amount of energy accumulated in the crack tip, which is the crack growth driving force.

Based on the above principle, when the internal residual stress in the thin film is more than the critical internal residual stress of crack growth, fine cracks will propagate in the thin film during the deposition process, reducing the barrier property of the film[20,21]. No matter how fine the crack is, WVTR can easily be affected, because any crack provides a path for moisture and oxygen molecules to penetrate into the thin film.

Figure 2f confirms that the TiO$_2$ film deposited at 40 °C had extremely lower residual stresses than the TiO$_2$ film deposited at a temperature higher than 55 °C. In addition, the residual stress in the film increased as the deposition temperature increased due to the more thermally activated desorption phenomenon. The TiO$_2$ film deposited at high temperature exhibited residual stresses of 200–300 MPa while the TiO$_2$ film deposited at 40 °C exhibited residual stresses of only about 20 MPa. Considering that the residual stresses in other ALD thin films have been reported to be several hundred MPa[17–20,22], the residual stress of the TiO$_2$ deposited at 40 °C is significantly low.

One of the major issues in the deposition process is the difference in the coefficient of thermal expansion (CTE). However, assuming that Al$_2$O$_3$ film is deposited on a Si wafer at 100 °C, the stress from the CTE difference is calculated to be only 20 MPa. The critical tensile stress of Al$_2$O$_3$ film is about 1.08 GPa when the elastic modulus of Al$_2$O$_3$ is considered to be 180 GPa[19,23]. Considering this, the stress from the difference in CTE is not critical. However, the residual stress in Al$_2$O$_3$ film has been measured to be 400–500 MPa[19], which is about half of the critical tensile stress. Therefore, the residual stress in the inorganic film, which can be on the order of several hundred MPa, needs to be carefully considered[22,23].

In summary, the TiO$_2$ was deposited most stably at a near-room-temperature of 40–55 °C, and when the process temperature was
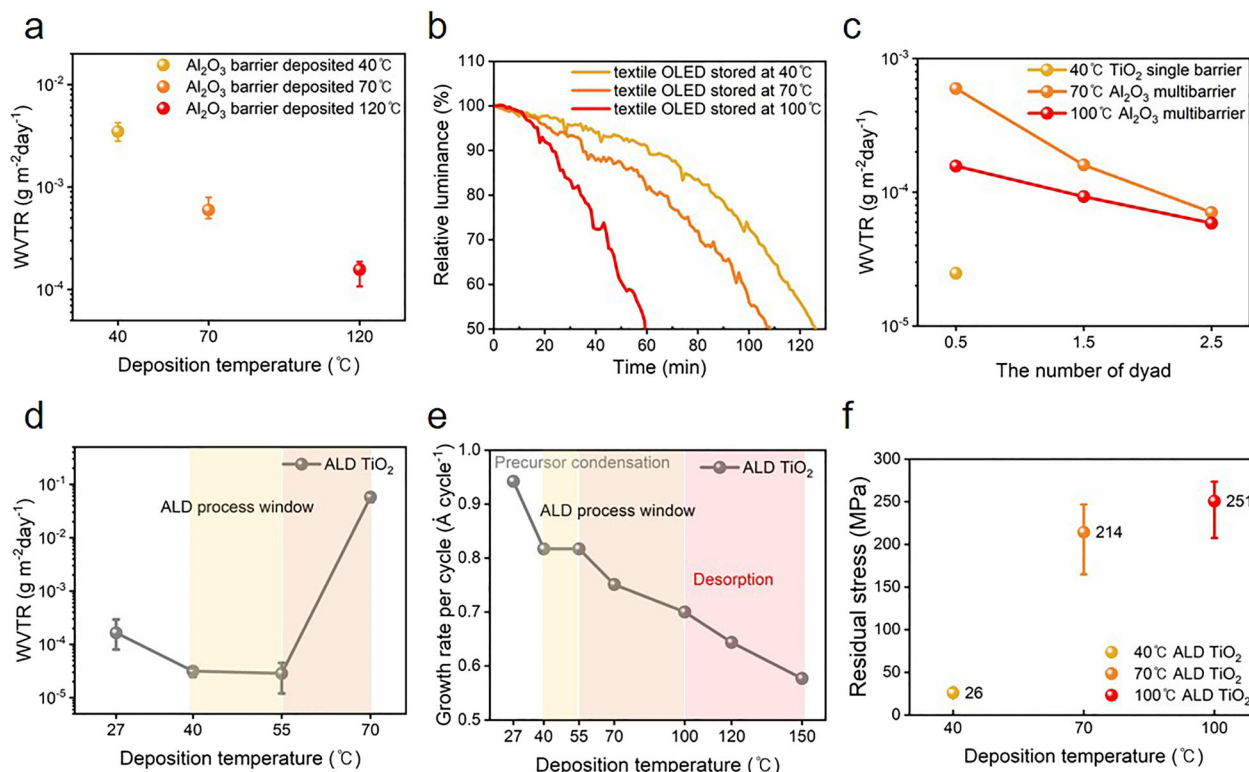
Fig. 2 WVTR of the ALD TiO$_2$ depending on the deposition temperature. a WVTR of the Al$_2$O$_3$ encapsulation layer depending on the deposition temperature. **b** Operating lifetime of the textile-based OLEDs depending on the storage temperature. **c** WVTR of the barriers depending on the deposition temperature and the number of dyads. **d** WVTR of the TiO$_2$ thin film depending on the deposition temperature. **e** ALD process window of TiO$_2$ thin film. **f** Residual stress in the TiO$_2$ thin film depending on the deposition temperature (with error bars that indicate standard deviation).

higher than 55 °C, precursor desorption occurred due to excessive thermal energy. Because of this phenomenon, the residual stress in the TiO$_2$ was lowest at a deposition temperature of 40–55 °C and increased when the process temperature was higher than 55 °C. The increased residual stress increased the WVTR of the TiO$_2$ because residual stress increases the crack driving force, G_{ss}, which promotes crack growth in the film. Therefore, the TiO$_2$ film exhibited the lowest WVTR at near-room-temperature deposition and the increased WVTR at higher process-temperature.

After chemically determining the encapsulation material based on the reaction mechanics of the precursors, the encapsulation structure was physically optimized. First, the overall barrier structure was designed as a nanolaminate structure to compensate for the low transmittance of the TiO$_2$ layer, and to decouple the cracks. Al$_2$O$_3$ was selected as the second laminate material because it is transparent and has good compatibility with the ALD process. As mentioned above, Al$_2$O$_3$ deposited at near-room-temperature, 40 °C, had poor barrier property due to its low film quality[9–11] (Fig. 1d). However, the crack decoupling effect of the nanolaminate structure was sufficient to overcome the poor barrier property of the Al$_2$O$_3$. The WVTR of the AT nanolaminate layer was improved compared to a TiO$_2$ single layer (Supplementary Fig. 3a).

The transmittance of the AT nanolaminate layer was improved by 6.35% compared to the single TiO$_2$ layer, because of the transparent Al$_2$O$_3$. The transmittance of a single TiO$_2$ layer was only 78.35% and the transmittance of an AT nanolaminate layer was 84.70%[24] (Supplementary Fig. 3b). The transmittance of the encapsulation barrier is important because it can cause luminance loss when applied to OLEDs[25].

Next, the sub-layer thickness of the AT nanolaminate layer was optimized to maximize the crack decoupling effect. The crack

decoupling effect is a phenomenon that increases the penetration path length of moisture and oxygen gas by decoupling the cracks in the thin film. The crack decoupling effect is maximized when the total barrier thickness is fixed and sub-layers are most repeatedly alternated within the nanolaminate barrier[26]; that is, it is when the sub-layers are alternatively deposited in the thinnest possible layer. If the sub-layer is too thin, it becomes a mixed alloy phase, not a nanolaminate phase. Therefore, the nanolaminate structure should be carefully designed. To identify the minimum thickness of sub-layers that can be distinguished as individual separate layers, thickness control was performed at the nanometer scale by the ALD deposition and the structure was confirmed through high-resolution transmission electron microscopy (TEM) analysis. The AT nanolaminate barriers were deposited by increasing the sub-layer thickness from 1.25 to 5 nm with the total barrier thickness fixed at 30 nm. Figure 3a shows that when the thickness of the sub-layer was 3 nm, it started to appear as a separate layer, and when the thickness was less than 2.1 nm, it became an alloy phase. These results indicated that the crack decoupling effect will be maximized when the sub-layer is deposited at 3 nm thickness. Figure 3a demonstrates that when the thickness of the sub-layer was 3 nm, the WVTR of the AT nanolaminate barrier was at its lowest, estimated to be 2.58×10^{-5} g m^{-2} day^{-1}.

In addition to the sub-layer thickness, the total barrier thickness needs to be carefully determined as well. It can be intuitively predicted that the WVTR decreases as the barrier thickness increases based on Fick's law, which is the diffusion equation of gas molecules[27]. However, the WVTR increases again when the thickness of the barrier exceeds a certain thickness, due to the accumulation of residual stress in the film, which is not considered in Fick's law. As the thickness of the film increases, residual stress
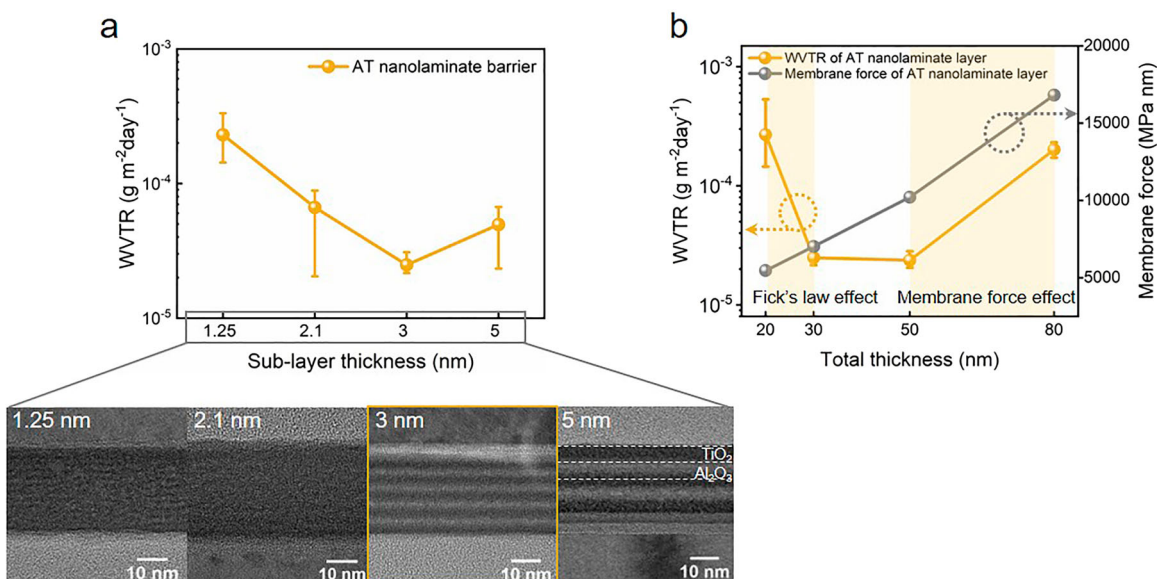
Fig. 3 Optimization of the encapsulation barrier structure. a TEM images and WVTRs of the Al_2O_3/TiO_2 nanolaminate layer (AT nanolaminate layer) with sub-layer thicknesses of 1.25, 2.1, 3, and 5 nm, respectively. Scale bar, 10 nm. **b** WVTR and membrane force of the AT nanolaminate barrier as a function of the total barrier thickness (with error bars that indicate standard deviation).

accumulates in the film, reducing the stability of the film. Figure 3b shows that the WVTR increased again when the thickness of the AT nanolaminate layer was more than 50 nm. It was also confirmed that as the total thickness of the film increased, the membrane force in the film increased proportionally. Consequently, the total barrier thickness was determined to be 30 nm, which was the optimum thickness in the WVTR saturation range between the region where Fick's law is dominant and the membrane force dominant region.

Finally, the structure and composition of the optimized AT nanolaminate layer was visualized through TEM and energy dispersive spectroscopy (EDS) measurements (Supplementary Fig. 3c).

Improvement in flexibility and waterproof property

A highly cross-linked pV3D3 polymer film was deposited via initiated chemical vapor deposition (iCVD) on the AT nanolaminate layer to improve the transmittance, mechanical flexibility, and waterproof property of the barrier for real wearable OLEDs. The pV3D3 organic layer has been reported to be an efficient organic layer for thin-film encapsulation (TFE) due to its flexible, smooth, dense, and hydrophobic characteristics[28–30]. In this study, the compressive residual stress and high chemical stability of the pV3D3 polymer layer was demonstrated and utilized.

The transmittance of the resulting bilayer encapsulation layer was estimated. The transparency of the encapsulation layer is extremely important because the OLED's light must pass through the encapsulation layer. The transmittance was measured to be 84.70% for the AT nanolaminate layer and 87.93% for the bilayer encapsulation layer (Supplementary Fig. 4a). Depositing the pV3D3 polymer layer onto the AT nanolaminate layer improved the transmittance by 3.23%. The improvement in transmittance was attributed to Fresnel reflection, which theoretically explains the behavior of light at an interface between media with different optical constants[25]. When a transmittance simulation based on the Fresnel transfer matrix was conducted, the results were the same as the experimental measurements (Supplementary Fig. 4b and Supplementary Fig. 4c).

Among the thin films in textile-based OLED, the encapsulation layer determines the flexibility of the overall structure because it contains fragile inorganic film to ensure effective barrier property.

Thus, it is important to improve the flexibility of encapsulation layer for increasing the durability of the textile-based OLEDs against deformation by the movement of a human body. When external deformation is applied to the barrier film, the total stress in the film is based not only on the external deformation stress, but also the internal residual stress[20,21]. Thus, if the internal residual stress in the barrier is controlled to zero, then the barrier film will be able to endure more external stress. The residual stress in the barrier can be controlled by offsetting the stress, using layers with opposite residual stresses, as shown in Fig. 4a.

It is known that cross-linking polymers deposited via the iCVD process experience compressive residual stress[31,32]. Figure 4b indicates that the pV3D3 thin film had a compressive residual stress of −77.78 MPa. The deposition temperature[33], deposition rate[34], and surface mobility[35] of the material during iCVD deposition are factors that contribute to the film stress. In solvent-based processes, which are widely used for synthesizing polymer film, it is hard to precisely control the residual stress of the film. In contrast, the residual stress in polymer films synthesized via the iCVD system are relatively reproducible and controllable. Control of the total film residual stress is particularly easy, since the iCVD system allows precise film thickness control. In this study, since the AT nanolaminate layer had an internal tensile stress of 230.40 MPa, the thickness of the pV3D3 film deposited on the AT nanolaminate layer was controlled to reduce the internal residual stress of the bilayer to zero.

The total residual stress of a multilayer is given by[19,22],

$$\sigma_{\text{total}} = \sigma_1 \cdot d_1 + \sigma_2 \cdot d_2 + \sigma_3 \cdot d_3 + \sigma_4 \cdot d_4 + \cdots + \sigma_n \cdot d_n \qquad (2)$$

where σ_n is the residual stress of the n_{th} layer, and d_n is the thickness of the n_{th} layer. Since the thickness of the AT nanolaminate layer was determined to be 30 nm through the structure optimization, the optimum thickness of the pV3D3 polymer film was calculated to be 85 nm according to the above Eq. (2). Figure 4b indicates that when the pV3D3 thin film was accurately controlled to 85 nm on the AT nanolaminate layer, the residual stress in the bilayer decreased to near zero. To confirm that this stress compensation improved the mechanical flexibility of the barrier, the WVTR of the bilayer was measured after tensile bending. Bending was conducted 1000 times for each strain. Figure 4c indicates that the critical strain of the AT nanolaminate
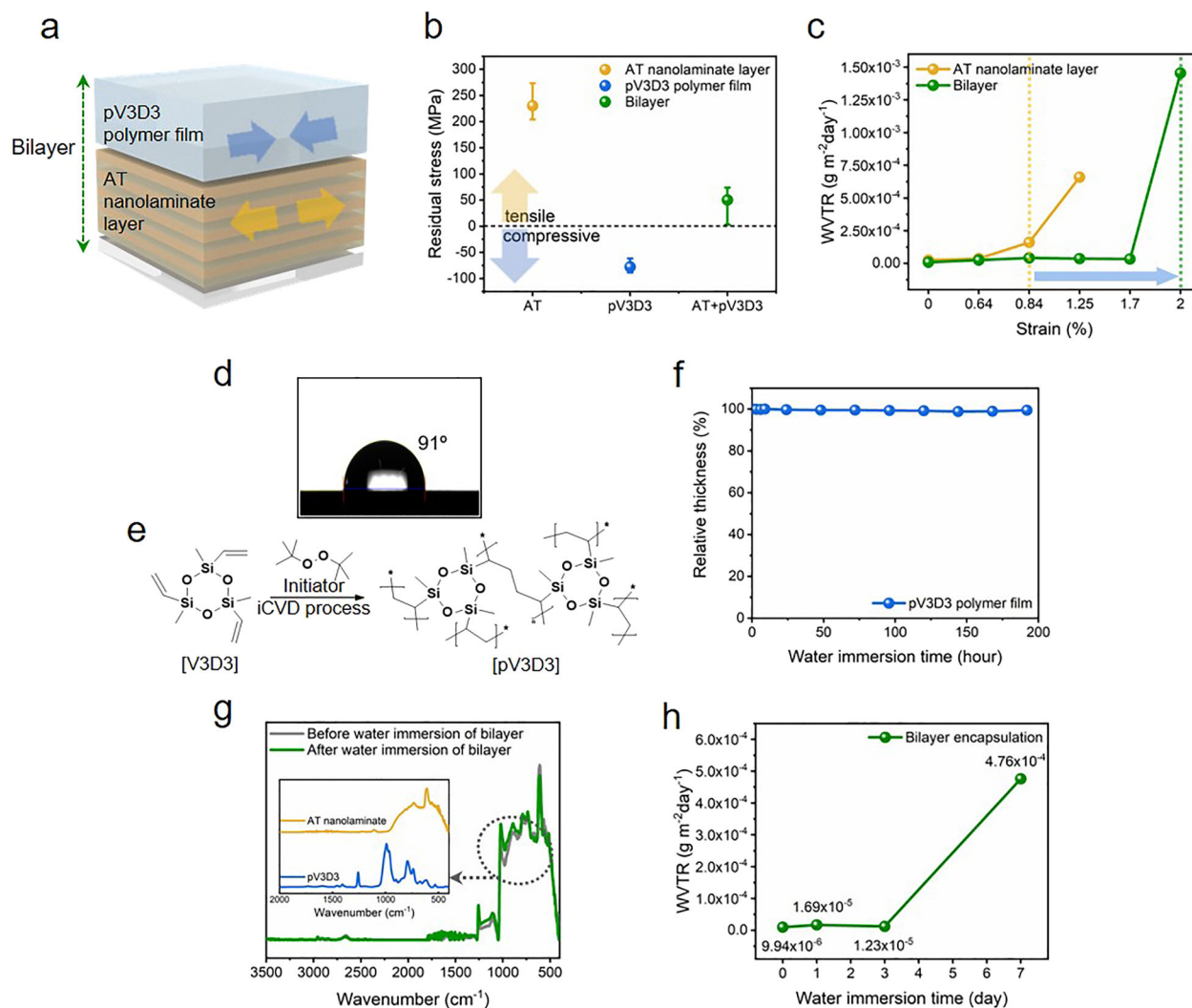
Fig. 4 Foldable and washable encapsulation layer. a Illustration of the method for controlling residual stress utilizing the residual stress in each layer. **b** Residual stress in the Al_2O_3/TiO_2 nanolaminate layer (AT nanolaminate layer), pV3D3 polymer film, and bilayer. **c** WVTR of the barriers after 1000 times bending as a function of bending strain. **d** Contact angle of the pV3D3 polymer film. **e** Chemical structure of the V3D3 monomer, initiator, and pV3D3 polymer. **f** Thickness of the pV3D3 polymer film as a function of water immersion time. **g** FT-IR spectra of the bilayer before/after water immersion for 10 days. **h** WVTR of the bilayer as a function of the dipping time (with error bars that indicate standard deviation).

layer where internal stress was not compensated was 0.84%, while the critical strain of the bilayer, where internal stress was compensated, improved to 2%. To ensure the reliability of the experiment, 3 or more encapsulation samples were estimated for each strain, and the results were averaged.

The pV3D3 thin film was also utilized as a capping layer to achieve a waterproof barrier, to allow the practical use of wearable OLEDs even with rain or washing. ALD oxide films have been reported to easily hydrolyze in water[36,37]. Therefore, a capping layer is essential to protect the AT nanolaminate layer. The capping layer should be hydrophobic and chemically stable to perform its capping role even after a long time in water[38,39].

The pV3D3 film is hydrophobic, and this was confirmed by water contact angle (WCA) analysis. Figure 4d reveals that the WCA of the pV3D3 film was 91°. When the outermost layer is hydrophobic, moisture molecules have difficulty absorbing on to the surface and are pushed away from the surface. Therefore, if the capping layer is hydrophobic, the encapsulation layer cannot be easily oxidized by water molecules, and it can preserve its WVTR, even in water. In addition, the flow of moisture into the encapsulation layer is reduced because the water molecules are

repelled from the surface. Consequently, the hydrophobic capping layer allows the encapsulation layer to survive washing.

Next, the chemical stability of the pV3D3 polymer was examined. pV3D3 polymer thin film has good chemical stability because of its high cross-linking density[28]. As shown in Fig. 4e, the 1,3,5-trimethyl-1,3,5-trivinylcyclotrisiloxane (V3D3) monomer has many cross-linking sites, so the pV3D3 polymer can be highly cross-linked. It was confirmed by Fourier-transform infrared spectroscopy (FTIR) analysis that most of the monomers were cross-linked during the iCVD process (Supplementary Fig. 4d). As shown in Fig. 4f, the pV3D3 polymer demonstrated its high chemical stability in water by showing that the thickness of the pV3D3 polymer was not changed even after 8 days in water. This result indicates that the pV3D3 polymer did not chemically dissolve in water, and retained its chemical properties, meaning the pV3D3 thin film can sufficiently protect the AT nanolaminate barrier from hydrolysis in water. To confirm this, FTIR analysis was performed again after the bilayer encapsulation was immersed in water for 10 days. Figure 4g indicates that the spectrum was exactly the same as that of the bilayer before immersion. As shown in Fig. 4h, the important WVTR increased by only 1 order,
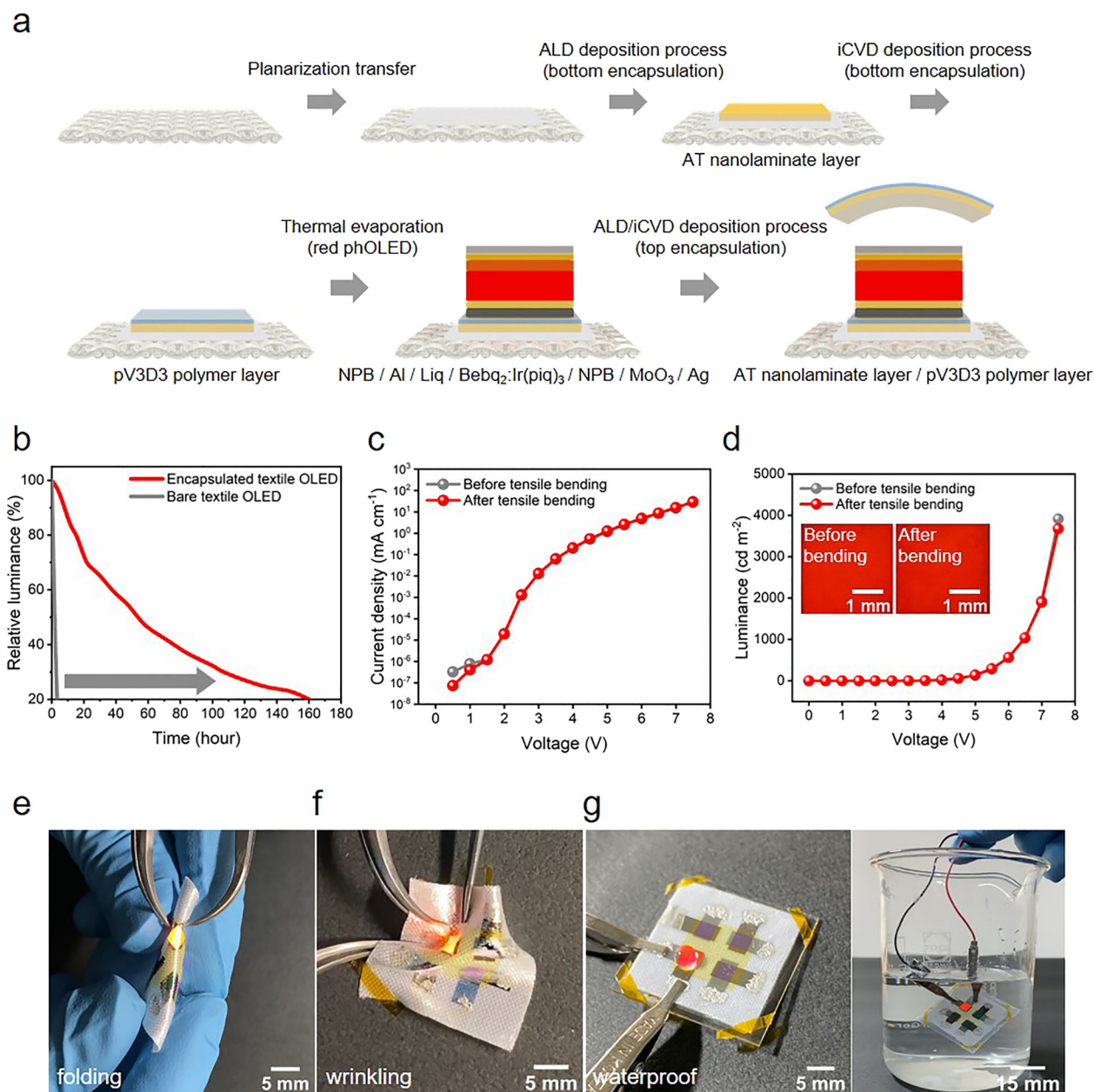
Fig. 5 Fabrication of textile-based OLEDs with bilayer encapsulation. a Fabrication process of the textile-based OLEDs. b Operating lifetime of the textile-based OLEDs with/without encapsulation. c J–V curves of the textile-based OLEDs after bending 1000 times with a 1.5 mm radius. d L–V curves and cell images (inset) of the textile-based OLEDs after bending 1000 times with a 1.5 mm radius. Scale bar, 1 mm. e Photograph of the textile-based OLED folded by hands. Scale bar, 5 mm. f Photograph of the textile-based OLED wrinkled by hands. Scale bar, 5 mm. g Photograph of the textile-based OLED immersed in water. Scale bar, 5 mm and 15 mm, respectively.

even after immersion in water for 7 days. Based on these results, it was confirmed that the barrier property was maintained in water, thereby making washable OLEDs possible.

Realization of a foldable and washable textile-based OLED

Figure 5a illustrates the entire fabrication process of the textile-based OLEDs. First, a planarization layer was transferred to make a smooth substrate surface for stable OLED deposition[40]. Then, in order to block moisture permeation from the textile substrate side, a bottom encapsulation process was performed, and an OLED was deposited by thermal evaporation. Finally, for complete OLED passivation from moisture and oxygen gas molecules, top encapsulation process was conducted.

To achieve waterproof wearable OLEDs in other studies, an attachable encapsulation using a sticky substrate or thick elastomer encapsulation have been utilized. However, such encapsulation processes are incompatible with the original texture of the fabric. In this study, wearable OLEDs were realized on a polyester textile using direct encapsulation. Supplementary Fig. 5a, b shows that after this fabrication process, there was no physical deterioration of the polyester textile substrate, such as rolling or shrinking or expansion. After the encapsulation process, there was also no change in the optoelectrical characteristics of the OLEDs due to the low temperature and short time of the encapsulation process.

Figure 5b compares the reliability of the wearable OLED in an ambient environment. The bare textile-based OLED, which was

not encapsulated, had an operating lifetime of only 6 h, but the textile-based OLED that was encapsulated showed an improved reliability of 160 h under an initial luminance of 1000 nit.

Next, external deformation was applied to the textile-based OLEDs to confirm their durability against mechanical deformation. To be wearable in daily life, the textile-based OLED should maintain their optoelectronic characteristics after repetitive mechanical deformation. Tensile bending was conducted 1000 times with a 1.5 mm radius, which represents a 1.7% tensile bending strain (Supplementary Fig. 5c). As shown in Fig. 5c, d and Supplementary Fig. 5d, the *J–V–L* curves and operating lifetime of the textile-based OLED were maintained after this repetitive bending deformation. Moreover, Fig. 5e, f shows that there was no physical cracking or delamination in the emission area, which fully continued to emit red light even when the devices were folded and wrinkled by hand. This confirms that the textile-based OLED can sufficiently endure external repetitive deformation such as bending, folding, or wrinkling, which are typical of the active movements of a human body.

In addition, to demonstrate waterproof property of the encapsulated OLEDs, the optoelectronic characteristics of OLEDs were estimated depending on water immersion time. The results showed that the bilayer-encapsulated OLEDs exhibited no deterioration of optoelectronic characteristics even after water immersion for 1440 min, confirming the encapsulation layer resulted in highly environmentally robust OLEDs (Supplementary Fig. 5e, f). To ensure the reliability of the experiment, a total of 6 OLED samples were estimated and the results were averaged. As shown in Fig. 5g, the textile-based OLED emitted red light even in water.

Finally, Supplementary Fig. 6 shows a wearable red OLED that was realized on a typical dress-shirt and T-shirt. These samples demonstrate the potential practical application by emitting red light with a luminance of 1000 nit, which is required for outdoor display, and displaying information such as a logo, the weather, time, or date. To operate the wearable OLED, a flexible battery that supplied 6 V to the OLED device was used. Therefore, the real wearable OLEDs were fabricated and showed the potential to realize the smart e-textiles.

A reliable, foldable, and washable textile-based OLED was fabricated and their practical usability was demonstrated. The main technology used to realize this textile-based OLED was a multi-functional near-room-temperature encapsulation layer. It was demonstrated that an ALD TiO$_2$ thin film deposited at near-room-temperature has outstanding impermeability and by this demonstration, a near-room-temperature encapsulation with WVTR on the order of 10^{-6} g m^{-2} day^{-1} was developed. To ensure mechanical flexibility and waterproof property, an internal stress analysis was performed, and a highly cross-linked iCVD polymer capping layer was introduced. After applying this barrier to the textile-based OLED, it exhibited an operating life-time of 160 h with an initial luminance of 1000 nit. The OLED maintained its optoelectronic characteristics and operating lifetime even after tensile bending 1000 times with a 1.5 mm radius, which is enough flexibility to endure the deformation by movement of human body. In addition, the bilayer-encapsulated OLEDs retained their initial optoelectronic characteristics even after immersion in water for 1440 min. These experimental results confirmed that the textile-based OLED can continue to operate despite water exposure such as washing or rain.

It is expected that these functional wearable OLEDs will play an important role in visualizing information on smart clothes for the IoTs in the future. In addition, TiO$_2$ material will be the main encapsulation material as an alternative to Al$_2$O$_3$, because of its high impermeability despite near-room-temperature deposition temperature. With the TiO$_2$ material, the proposed encapsulation barrier provides possibility to improve the reliability of all types of flexible substrates and devices that are extremely sensitive to temperature or moisture.

METHODS

Encapsulation fabrication

The encapsulation barrier was fabricated as a bilayer structure that consisted of an inorganic layer and an organic layer. Al$_2$O$_3$ and TiO$_2$ materials were utilized for the inorganic layer. For the organic layer, pV3D3 was utilized. pV3D3 was deposited via iCVD. To measure the WVTR values, an electrical calcium test was utilized.

OLEDs fabrication

Red phosphorescent OLEDs were fabricated on a polyester textile substrate on which the planarization layer and the bottom encapsulation barrier were deposited[40]. The following structure was utilized: Al (100 nm)/ Liq (1 nm)/Bebq$_2$:Irpiq$_3$ (70 nm)/NPB (62 nm)/MoO$_3$ (5 nm)/Ag (30 nm).

More details about experimental methods are provided in the Supplementary information.

REFERENCES

1. Jeon, Y. et al. A wearable photobiomodulation patch using a flexible red-wavelength OLED and its in vitro differential cell proliferation effects. *Adv. Mater. Technol.* **3**, 1–10 (2018).
2. Jeon, Y. et al. Sandwich-structure transferable free-form OLEDs for wearable and disposable skin wound photomedicine. *Light Sci. Appl.* **8**, 1–15 (2019).
3. Lee, H. et al. Toward all-day wearable health monitoring: an ultralow-power, reflective organic pulse oximetry sensing patch. *Sci. Adv.* **4**, 1–9 (2018).
4. Kwon, S. et al. Weavable and highly efficient organic light-emitting fibers for wearable electronics: a scalable, low-temperature process. *Nano Lett.* **18**, 347–356 (2018).
5. Kim, W. et al. Reliable actual fabric-based organic light-emitting diodes: toward a wearable display. *Adv. Electron. Mater.* **2**, 1–7 (2016).
6. Chen, N. et al. Low substrate temperature encapsulation for flexible electrodes and organic photovoltaics. *Adv. Energy Mater.* **5**, 1401442 (2015).
7. Wang, H. et al. Hermetic seal for perovskite solar cells: an improved plasma enhanced atomic layer deposition encapsulation. *Nano Energy* **69**, 104375 (2020).
8. Jeong, E. G., Kwon, J. H., Kang, K. S., Jeong, S. Y. & Choi, K. C. A review of highly reliable flexible encapsulation technologies towards rollable and foldable OLEDs. *J. Inf. Disp.* **21**, 19–32 (2019).
9. Groner, M. D., Fabreguette, F. H., Elam, J. W. & George, S. M. Low-temperature Al$_2$O$_3$ atomic layer deposition. *Chem. Mater.* **16**, 639–645 (2004).
10. Kukli, K., Ritala, M., Aarik, J., Uustare, T. & Leskelä, M. Influence of growth temperature on properties of zirconium dioxide films grown by atomic layer deposition. *J. Appl. Phys.* **92**, 1833–1840 (2002).
11. Bao, Y., Laitinen, M., Sajavaara, T. & Savin, H. Ozone-based atomic layer deposition of Al$_2$O$_3$ from dimethylaluminum chloride and its impact on silicon surface passivation. *Adv. Electron. Mater.* **3**, 1–7 (2017).
12. Xie, Q. et al. Atomic layer deposition of TiO$_2$ from tetrakis-dimethyl-amido titanium or Ti isopropoxide precursors and H$_2$O. *J. Appl. Phys.* **102**, 83521 (2007).
13. Xie, Q. et al. Growth kinetics and crystallization behavior of TiO$_2$ films prepared by plasma enhanced atomic layer deposition. *J. Electrochem. Soc.* **155**, H688 (2008).
14. Rentrop, S. et al. Atomic layer deposition of TiO$_2$ from tetrakis(dimethylamino) titanium and H$_2$O. *Thin Solid Films* **545**, 176–182 (2013).
15. Xie, Q. et al. Atomic layer deposition of TiO$_2$ from tetrakis-dimethyl-amido titanium or Ti isopropoxide precursors and H$_2$O. *J. Appl. Phys.* **102**, 83521 (2007).
16. Malet, P. & Munuera, G. Temperature-programmed desorption study of activated chemisorption involving a precursor state: desorption of water from TiO$_2$. *J. Chem. Soc. Faraday Trans.* **85**, 4157–4166 (1989).
17. Zhu, Z., Salmi, E. & Virtanen, S. Residual stress study of thin films deposited by atomic layer deposition. *Proc. Int. Conf. ASIC* **118**, 85501 (2017).

18. Ylivaara, O. M. E. et al. Aluminum oxide from trimethylaluminum and water by atomic layer deposition: the temperature dependence of residual stress, elastic modulus, hardness and adhesion. *Thin Solid Films* **552**, 124–135 (2014).

19. Behrendt, A. et al. Stress management in thin-film gas-permeation barriers. *ACS Appl. Mater. Interfaces* **8**, 4056–4061 (2016).

20. Bulusu, A. et al. Engineering the mechanical properties of ultrabarrier films grown by atomic layer deposition for the encapsulation of printed electronics. *J. Appl. Phys.* **118**, 85501 (2015).

21. Kim, K. et al. Optimizing crack onset strain for silicon nitride/fluoropolymer nanolaminate barrier films. *ACS Appl. Nano Mater.* **2**, 2525–2532 (2019).

22. Liu, H., Jensen, L., Ma, P. & Ristau, D. Stress compensated anti-reflection coating for high power laser deposited with IBS SiO_2 and ALD Al_2O_3. *Appl. Surf. Sci.* **476**, 521–527 (2019).

23. Jen, S. H., George, S. M., McLean, R. S. & Carcia, P. F. Alucone interlayers to minimize stress caused by thermal expansion mismatch between Al_2O_3 films and Teflon substrates. *ACS Appl. Mater. Interfaces* **5**, 1165–1173 (2013).

24. Kim, L. H. et al. Optimization of Al_2O_3/TiO_2 nanolaminate thin films prepared with different oxide ratios, for use in organic light-emitting diode encapsulation, via plasma-enhanced atomic layer deposition. *Phys. Chem. Chem. Phys.* **18**, 1042–1049 (2016).

25. Park, K. W. et al. High-performance thin H:SiON OLED encapsulation layer deposited by PECVD at low temperature. *RSC Adv.* **9**, 58–64 (2019).

26. Kwon, J. H. et al. Functional design of highly robust and flexible thin-film encapsulation composed of quasi-perfect sublayers for transparent, flexible displays. *ACS Appl. Mater. Interfaces* **9**, 43983–43992 (2017).

27. Seo, S.-W., Jung, E., Lim, C., Chae, H. & Cho, S.M. Moisture permeation through ultrathin TiO_2 films grown by atomic layer deposition. *Appl. Phys. Express* **5**, 035701 (2012).

28. Moon, H. et al. Synthesis of ultrathin polymer insulating layers by initiated chemical vapour deposition for low-power soft electronics. *Nat. Mater.* **14**, 628–635 (2015).

29. Kim, B. J. et al. A single-chamber system of initiated chemical vapor deposition and atomic layer deposition for fabrication of organic/inorganic multilayer films. *Adv. Eng. Mater.* **19**, 1–9 (2017).

30. Lee, Y. I. L. et al. A low-temperature thin-film encapsulation for enhanced stability of a highly efficient perovskite solar cell. *Adv. Energy Mater.* **8**, 1–8 (2018).

31. Lepró, X. et al. Ultralow stress, thermally stable cross-linked polymer films of polydivinylbenzene (PDVB). *Langmuir* **33**, 5204–5212 (2017).

32. Tenhaeff, W. E., Arora, W. J., Barbastathis, G. & Gleason, K. K. Integration of reactive polymeric nanofilms into a low-power microelectromechanical switch. *AIChE Annu. Meet. Conf. Proc.* **18**, 97–102 (2008).

33. Abermann, R. Measurements of the intrinsic stress in thin metal films. *Vacuum* **41**, 1279–1282 (1990).

34. Hearne, S. J. & Floro, J. A. Mechanisms inducing compressive stress during electrodeposition of Ni. *J. Appl. Phys.* **97**, 14901 (2005).

35. Chason, E. et al. Stress evolution during growth of 1-D island arrays: kinetics and length scaling. *Scr. Mater.* **97**, 33–36 (2015).

36. Jeong, E. G., Jeon, Y., Cho, S. H. & Choi, K. C. Textile-based washable polymer solar cells for optoelectronic modules: toward self-powered smart clothing. *Energy Environ. Sci.* **12**, 1878–1889 (2019).

37. Kim, L. H. et al. Al_2O_3/TiO_2 nanolaminate thin film encapsulation for organic thin film transistors via plasma-enhanced atomic layer deposition. *ACS Appl. Mater. Interfaces* **6**, 6731–6738 (2014).

38. Idígoras, J. et al. Enhancing moisture and water resistance in perovskite solar cells by encapsulation with ultrathin plasma polymers. *ACS Appl. Mater. Interfaces* **10**, 11587–11594 (2018).

39. Wang, L. et al. Enhanced moisture barrier performance for ALD-encapsulated OLEDs by introducing an organic protective layer. *J. Mater. Chem. C* **5**, 4017–4024 (2017).

40. Choi, S. et al. Multi-directionally wrinkle-able textile OLEDs for clothing-type displays. *npj Flex. Electron.* **4**, 1–9 (2020).

AUTHOR CONTRIBUTIONS
S. Y.J. and K.C.C. conceived and designed the research. S.Y.J. and H.R.S. mainly conducted the experiments and analyses, and prepared figures and the manuscript. Y.N. and H.-E.C. contributed to experiments about planarization of the textile substrate. K.S.K., Y.J., S.C., E. G.J. and J.H.K. designed the research object and specific experimental methods. Y.C.P. contributed to fabrication of the polymer film. J.L. contributed to optical simulation. S.G.I. provided useful advice throughout the research.

COMPETING INTERESTS
The authors declare no competing interests.

ADDITIONAL INFORMATION
Supplementary information The online version contains supplementary material available at https://doi.org/10.1038/s41528-021-00112-0.

Correspondence and requests for materials should be addressed to S.G.I. or K.C.C.

Reprints and permission information is available at http://www.nature.com/reprints

Publisher's note Springer Nature remains neutral with regard to jurisdictional claims in published maps and institutional affiliations.